

## Additional evidence of nuclear emissions during acoustic cavitation

R. P. Taleyarkhan,<sup>1,\*</sup> J. S. Cho,<sup>2</sup> C. D. West, R. T. Lahey, Jr.,<sup>3</sup> R. I. Nigmatulin,<sup>4</sup> and R. C. Block<sup>3</sup>

<sup>1</sup>*Purdue University, West Lafayette, Indiana 47907, USA*

<sup>2</sup>*Oak Ridge Associated Universities, Oak Ridge, Tennessee 37830, USA*

<sup>3</sup>*Rensselaer Polytechnic Institute, Troy, New York 12180, USA*

<sup>4</sup>*Russian Academy of Sciences, 6 Karl Marx Street, Ufa 450000, Russia*

(Received 13 May 2003; published 22 March 2004)

Time spectra of neutron and sonoluminescence emissions were measured in cavitation experiments with chilled deuterated acetone. Statistically significant neutron and gamma ray emissions were measured with a calibrated liquid-scintillation detector, and sonoluminescence emissions were measured with a photomultiplier tube. The neutron and sonoluminescence emissions were found to be time correlated over the time of significant bubble cluster dynamics. The neutron emission energy was less than 2.5 MeV and the neutron emission rate was up to  $\sim 4 \times 10^5$  n/s. Measurements of tritium production were also performed and these data implied a neutron emission rate due to D-D fusion which agreed with what was measured. In contrast, control experiments using normal acetone did not result in statistically significant tritium activity, or neutron or gamma ray emissions.

DOI: 10.1103/PhysRevE.69.036109

PACS number(s): 89.90.+n

### INTRODUCTION

The intense implosive collapse of bubbles, including acoustic cavitation bubbles, can lead to extremely high compressions and temperatures, and to the generation of light flashes attributed to sonoluminescence (SL). The modeling and analyses of the basic physical phenomena associated with such a process have been discussed elsewhere [1] and the key phenomena are depicted schematically in Fig. 1. Figure 1(a) shows the start of bubble implosion, during the compression phase of the impressed acoustic pressure field, when the gas/vapor Mach number is much less than unity. As the interfacial Mach number approaches unity a compression shock wave is formed in the gas/vapor mixture and, as shown schematically in Fig. 1(b), this shock wave (dashed line) moves toward the center of the bubble and, in doing so, intensifies. Figure 1(c) shows the situation just after the shock wave has bounced off itself at the center of the bubble which highly compresses and heats a small core region near the center of the bubble. At this point we normally have a SL light pulse, and if we have a suitable (e.g., deuterated) liquid in which the bubble temperatures, density and their duration are large enough, we may also have conditions suitable for nuclear emissions (i.e., nuclear fusion). Interestingly, these emissions and the pressurization process continue until a short time later when the interface comes to rest [see Fig. 1(d)]. Figure 1(e) shows the onset of bubble expansion during the rarefaction phase of the impressed acoustic pressure field, and Fig. 1(f) shows that a relatively weak shock wave is formed in the liquid surrounding the bubble during bubble expansion. As will be described later, for sufficiently violent implosions of relatively large bubbles this shock wave is normally heard by the experimenters after it reaches the wall of the test section in which the experiment is being per-

formed. Our aim was to study the ultrahigh compression effects and temperatures in vapor bubbles nucleated in highly tensioned liquids by means of fast neutrons, whereby the bubble radius increases from an initial radius ( $R_0$ ) of tens of nanometers to a maximum radius ( $R_m$ ) in the millimeter range. This results in a related volumetric expansion ratio which is huge [1] compared to that obtainable in conventional SL experiments (where  $R_m \sim 10R_0$ ). Such an ap-

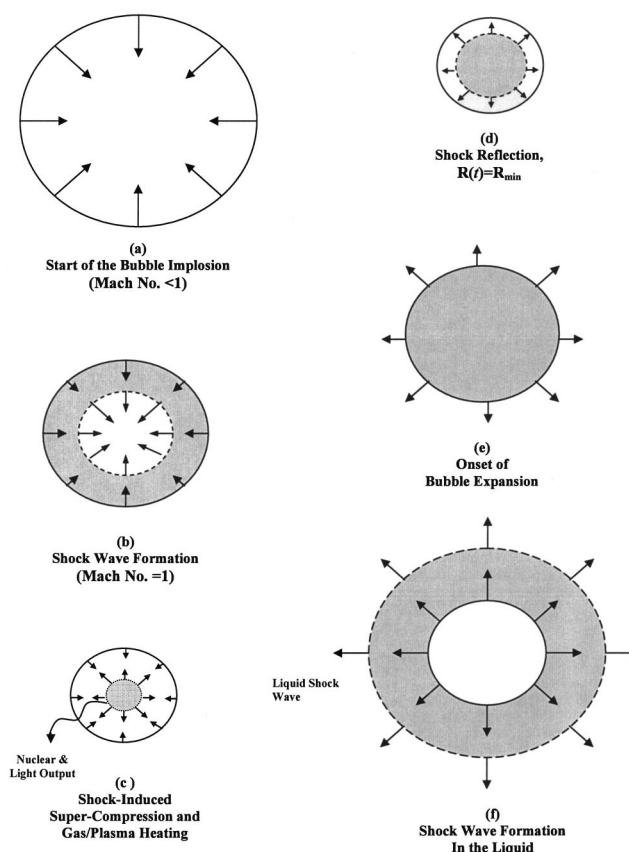


FIG. 1. Various stages of bubble implosion and shock-induced compression.

\*Also at Oak Ridge National Laboratory, Oak Ridge, TN, USA.

Author to whom correspondence should be addressed. Email address: rusi@purdue.edu

proach, with its vastly increased energy concentration potential during implosions, gives rise to very much higher peak temperatures and densities within the imploding bubbles, possibly leading to DD fusion and detectable levels of nuclear particle emissions in suitable deuterated liquids. Indeed, we have previously presented evidence [1] for neutron emission and tritium production during cavitation experiments with chilled deuterated acetone.

Comments received [2–6] on the previously published results [1] suggested the need for improved instrumentation and data gathering; for enhancing our understanding of the timing and rates of neutron and gamma ray emission activity; for improving the efficiency for the detection of neutron emissions during bubble implosions; and for addressing the potential for significant chemical effects from cavitation in the tritium measurements. Specifically, in the data presented previously [1], time spectra were obtained only for the period corresponding to the first implosion of the nucleated bubbles. In this paper, we report results of investigations using improved and additional instrumentation. These additional data fully support our previous results and provide complementary evidence of nuclear emissions from cavitating chilled deuterated acetone that are indicative of deuterium-deuterium (DD) fusion.

## EXPERIMENTAL SYSTEM

The experimental test apparatus [Fig. 2(a)] was kept similar to that used for the results reported previously [1]. The test liquid was placed in an approximately cylindrical Pyrex glass test section and driven acoustically with a lead-zirconate-titanate (PZT) piezoelectric driver ring attached to the outside surface of the test section. This induced an acoustic standing wave in the test section with a pressure antinode of amplitude  $\sim \pm 15$  bar. A new liquid scintillator (LS) detection system was set up for pulse-shape discrimination (PSD), and was used for the detection of neutron and gamma ray signals with the instrumentation shown in Fig. 2(b). As compared to the data acquisition system used earlier [1], the new system [7] includes fast multichannel scaling (MCS) capability that could be used to obtain time spectra of the neutron and SL signals over the entire time span of experimentation. A multichannel analyzer (MCA), operated in the pulse height mode, was used to obtain pulse height data with and without gating, and also for gating of gamma ray signals.

In the experimentally observed sequence of events [Fig. 2(c)], neutrons from a pulse neutron generator (PNG) nucleated bubbles in the tensioned liquid when the cavitation threshold was exceeded at the time of the PNG neutron burst. Thereafter, the vapor bubbles grew until increasing pressure in the liquid during the second half of the acoustic cycle caused them to collapse. If the collapse was robust enough (i.e., an implosion occurred), the bubble emitted a SL flash which was detected by a photomultiplier tube (PMT) [7]. If the vapor contains sufficient deuterium (D) atoms, and the conditions are appropriate for DD fusion, nuclear particles (neutrons and gamma rays) would be emitted and seen in the response of the LS detector. Subsequent to the first implo-

sion, the bubble cloud may undergo periodic growth and energetic collapses at the 19.3 kHz frequency of the forcing acoustic pressure field. This process is repeated until the bubbles condense, and there can be neutron and gamma ray emissions during the subsequent implosions, however, the yield can differ from that during the initial implosion. Shown in Fig. 2(d) are typical photographic images of bubble clouds taken 1 ms apart in acetone at  $\sim 3^\circ\text{C}$ . It is seen that the bubble clouds persist in the pressure antinode of the test section for  $\sim 5$  ms prior to condensing, and reach bubble cloud sizes in the range of  $\sim 6$  mm in diameter.

The liquid was first degassed, as reported on previously [1], by acoustically cavitating the liquid under vacuum ( $\sim 10$  kPa) with neutrons for  $\sim 2$  h. This process is important since gassy vapor bubbles do not exhibit the desired intense implosive collapse characteristics as clearly evidenced from shock traces measured by microphone signals. Subsequent to degassing the liquid, the PNG was operated at  $\sim 200$  Hz (i.e., at a rate 100 times smaller than the acoustic driving frequency) during which neutrons were emitted over a time span of  $\sim 15$   $\mu\text{s}$  [ $\sim 6$ – $7$   $\mu\text{s}$  full width at half maximum (FWHM)]. The PNG burst was initiated when the liquid tension was greatest (i.e., at  $-15$  bar). For these conditions a bubble cloud was formed and rapidly expanded. Later, when the impressed acoustic pressure increases, it imploded emitting a burst of closely spaced SL flashes over an  $\sim 15$ – $20$   $\mu\text{s}$  time interval (each of  $\sim 5$  ms duration).

## LIQUID SCINTILLATION (LS) DETECTOR CALIBRATION

Careful calibration of the response of the LS detector was conducted using gamma rays from Cs-137 and Co-60 sources, 14 MeV neutrons from a PNG, and emissions from a plutonium-beryllium (Pu-Be) isotope source. The results of these calibrations are shown in Fig. 3(a). The pulse height spectra for Cs-137 and Co-60 are also shown on a stretched scale in the lower plot; a relatively sharp Compton edge results from the monoenergetic  $\sim 0.67$  MeV gamma ray emission from Cs-137, whereas, a somewhat broader edge results for Co-60 due to the two closely-spaced 1.17 and 1.33 MeV gamma rays. Note also that the Pu-Be source exhibited the well-known 4.4 MeV Compton edge associated with the deexcitation  $^{12}\text{C}^*$  gamma ray. The pulse height response of the LS detector matched the well accepted light output for EJ-301/NE-213 type detectors [8,9]. The  $\sim 2.5$  MeV proton recoil edge is known [10] to lie between the Compton edges for gamma rays from Cs-137 and Co-60. Moreover, the ratio of light output for 14 MeV neutrons to that for 2.5 MeV neutrons was found to be  $\sim 11.7$  as expected [10]. Using a Pu-Be source with a known neutron emission rate, the net efficiency for the detection of fast (mainly  $< 4$  MeV) neutrons was estimated [11] to be  $\sim 6 \times 10^{-4}$ . Figure 3(b) displays time spectra of gamma and neutron signals with and without pulse shape discrimination (PSD). For PSD the discriminator settings were chosen to reject more than 95% of

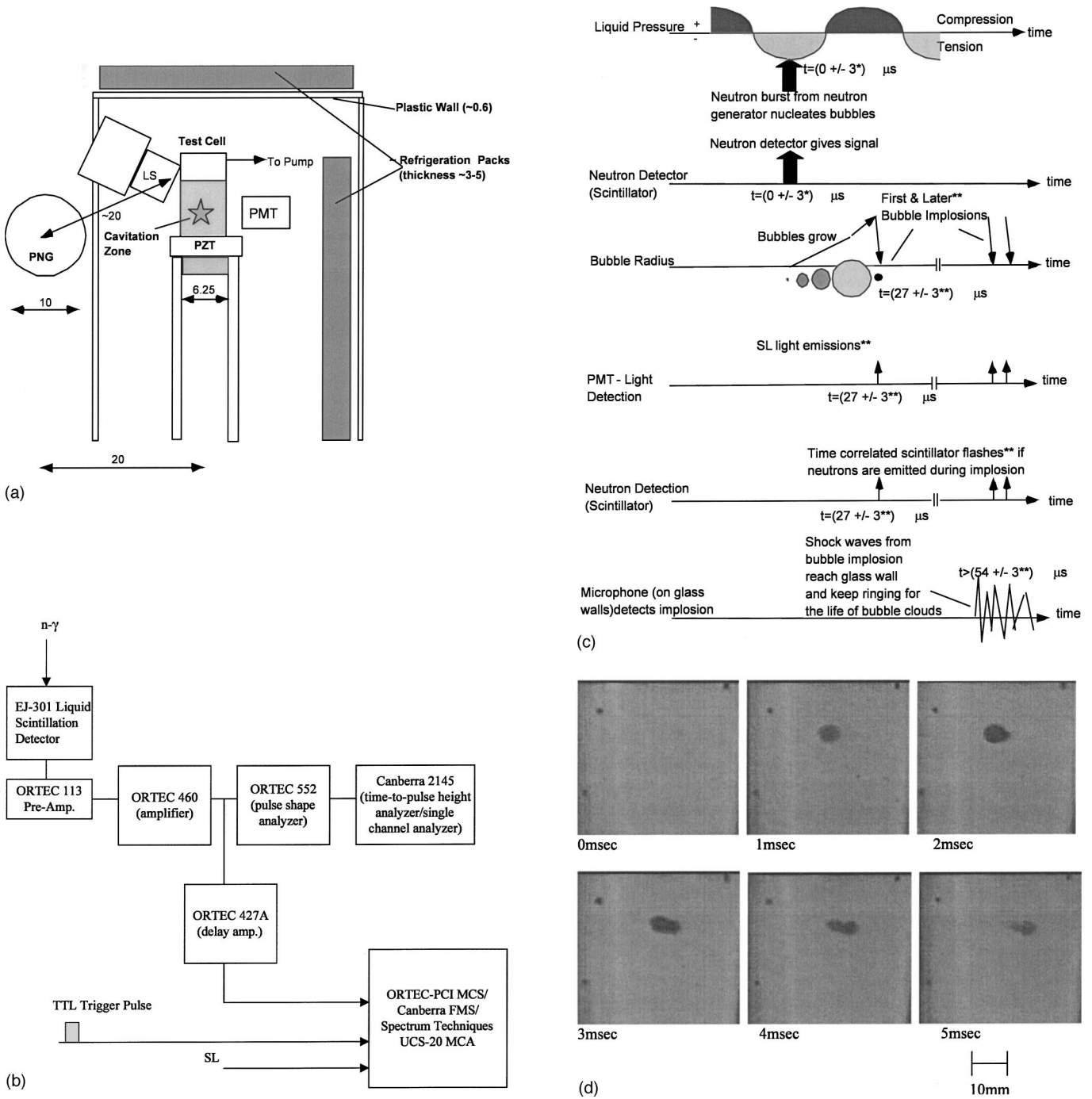


FIG. 2. (a) Schematic arrangement of test chamber and key components [Notes: (1) All dimensions are in cm; (2) acronyms: LS (liquid scintillation detector); PNG (pulse neutron generator); PMT (photomultiplier tube for SL detection); (3) borated shield blocks, furniture, etc. not shown]. (b) Sample layout of electronic components for pulse-shape discrimination and time spectra data acquisition. (c) Time sequence of events. (\*) Full width at half maximum; (\*\*) can continue for several cycles (to ~5 ms at 0 °C). (d) Images of bubble cloud nucleation to collapse for tests with  $\text{C}_3\text{H}_6\text{O}$  (3 °C). (Images taken at rate of 1000 frames per second and 1/2000 second shutter speed.)

the gamma rays. As expected [9], the fractional counts associated with the gamma rays was found to be ~45% of the total counts in the time spectrum for the Pu-Be source. In addition, the LS detector was carefully calibrated with monoenergetic neutrons at the RPI LINAC, and these calibrations agreed very well with the *in situ* ORNL calibrations discussed above.

### EXPERIMENTAL OBSERVATIONS FOR $\text{C}_3\text{H}_6\text{O}$ AND $\text{C}_3\text{D}_6\text{O}$

We conducted experiments with standard acetone,  $\text{C}_3\text{H}_6\text{O}$  (100 atom% pure), and deuterated acetone,  $\text{C}_3\text{D}_6\text{O}$  (certified 99.92 atom% D-acetone), filtered before use through 1  $\mu\text{m}$  filters. Degassing and other aspects of the forcing pressure amplitude were kept the same as for the conditions reported

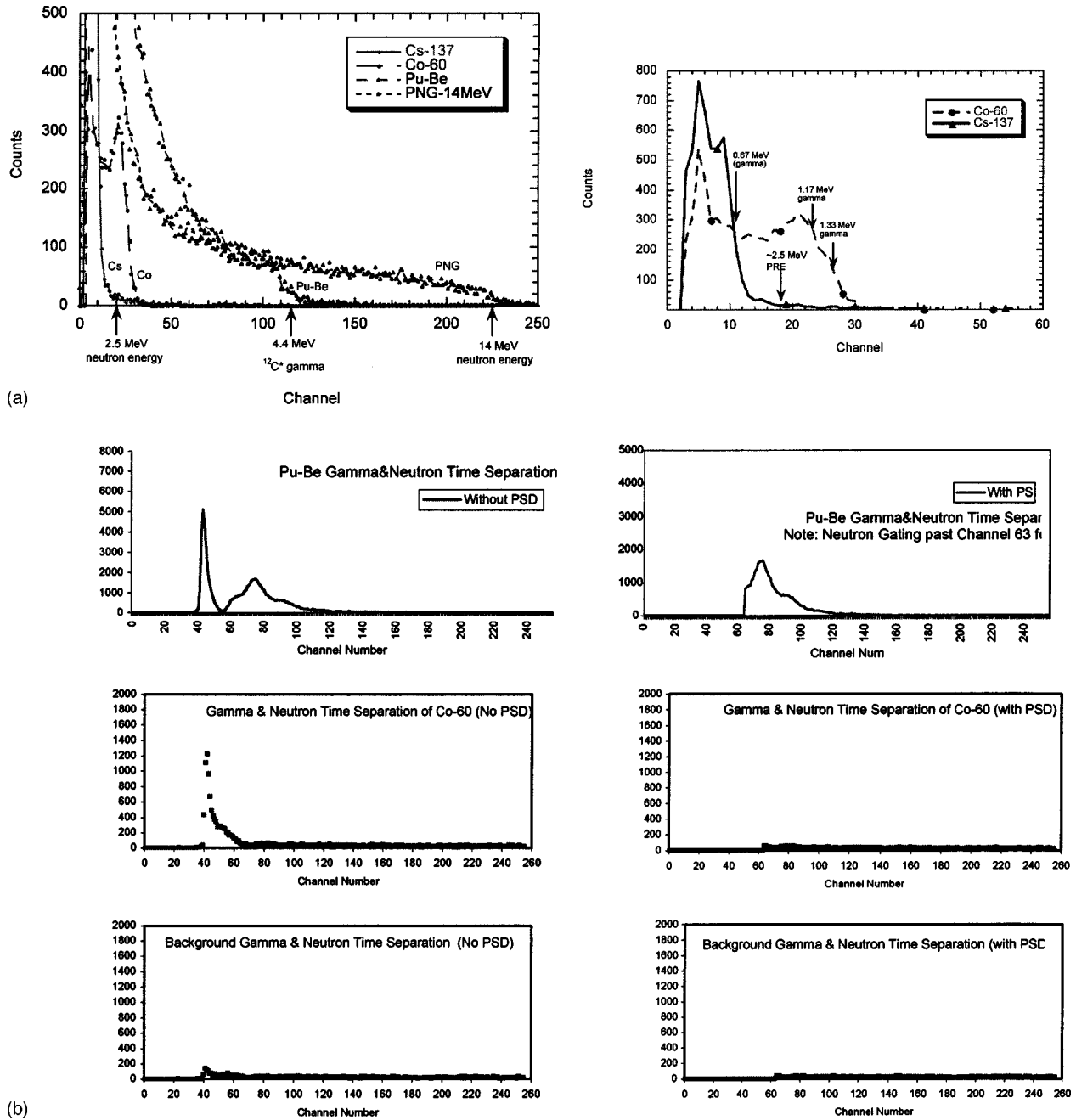


FIG. 3. (a) LS detector pulse height spectra. (b) Time-spectra data with and without PSD for Pu-Be source, Co-60 monoenergetic gamma source, and background. For Pu-Be source the gamma ray fraction is  $\sim 40\%$  of the total counts obtained.

previously [1]. The pressure amplitude at the acoustic pressure antinode in our test section was maintained at a nominal value of  $\sim \pm 15$  bar.

**NEUTRON AND SL SPECTRA DATA ACQUISITION**

We used well-established pulse shape discrimination (PSD) techniques in experiments with and without cavitation to check for neutron production and time correlations with SL emission data. Time spectra were obtained using 1000 channel MCS boards with  $5 \mu\text{s}$  dwell times, such that the neutron counts during PNG operation, which occur within the first  $25 \mu\text{s}$  after the trigger signal is transmitted to the

PNG, are well separated from the signals during subsequent events all the way to  $5000 \mu\text{s}$ , which is just before the next PNG trigger pulse was transmitted. It was verified that, for identical settings without cavitation, the collective PNG neutron output of counts over 50 s duration was stable and varied by only  $\sim \pm 1\%$  from measurement to measurement. Time spectra data were collected and statistically significant counts were obtained. Representative neutron and SL time spectra are shown in Figs. 4 through 7.

Figure 4 shows the MCS cumulative neutron count spectra vs time after the PNG fires for tests with  $\text{C}_3\text{D}_6\text{O}$ . These spectra were accumulated for 10000 sweeps, each of 5 ms duration. Figure 4(a) is with cavitation while Fig. 4(b) is

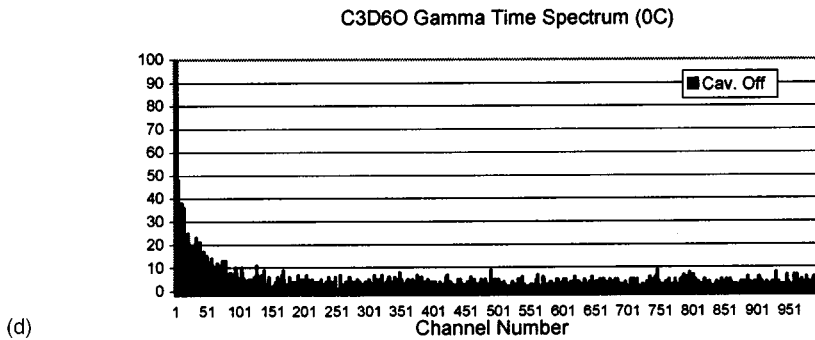
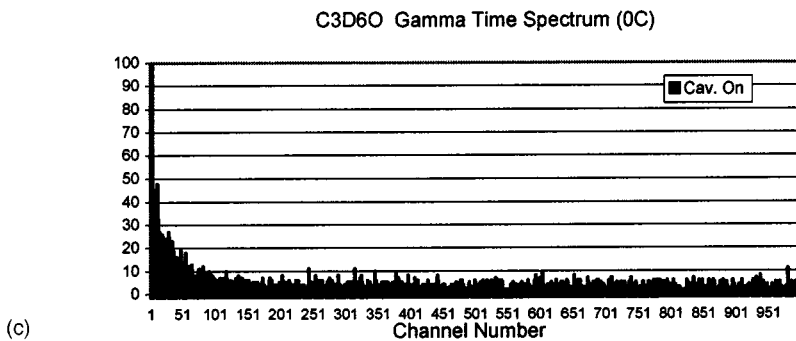
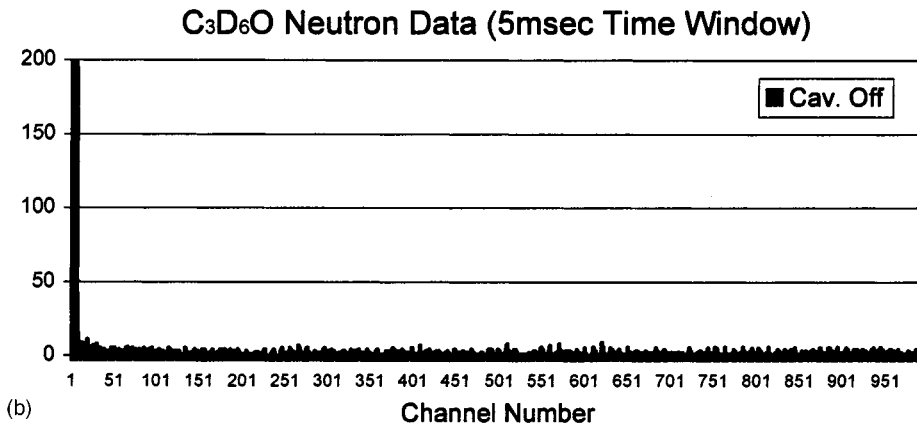
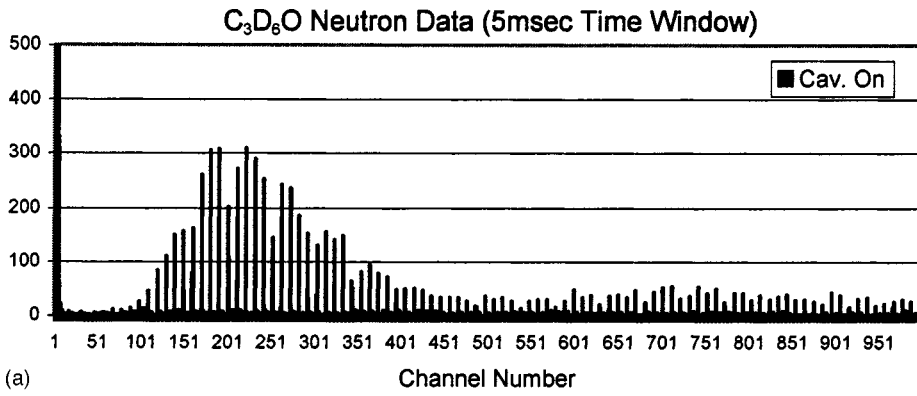


FIG. 4. (a) Time spectrum of neutron counts for tests with cavitation on (C<sub>3</sub>D<sub>6</sub>O at 0 °C; PNG drive frequency ~200 Hz; acoustic forcing frequency = ~19.3 kHz; time channel width = 5 μs). (b) Time spectrum of neutron counts for tests with cavitation off (C<sub>3</sub>D<sub>6</sub>O at 0 °C; PNG drive frequency ~200 Hz; PZT drive left on but frequency phase shifted to prevent cavitation; time channel width = 5 μs). (c) Time spectrum of gamma ray counts for tests with cavitation on (C<sub>3</sub>D<sub>6</sub>O at 0 °C; PNG drive frequency ~200 Hz; acoustic forcing frequency = ~19.3 kHz; time channel width = 5 μs). (d) Time spectrum of gamma ray counts for tests with cavitation off (C<sub>3</sub>D<sub>6</sub>O at 0 °C; PNG drive frequency ~200 Hz; PZT drive left on but frequency phase shifted to prevent cavitation; time channel width = 5 μs).

without. It can be seen that excess neutrons were only detected when there were cavitation bubbles. It is interesting to note in Figs. 4(a) and 7(a) that there is a significant peak during the implosion associated with the first sonic cycle of period 52 μs, which occurs about 20 μs after the PNG neutrons emanate, and then there appears a time span of low

neutron counts extending to channel ~100 (~500 μs) which is ~10 acoustic cycles. Starting at channel ~100 (500 μs) the neutron counts start to grow significantly to a peak near channel ~180 (~900 μs) and then asymptotically decrease to a lower level around channel ~500 (2 500 μs), reaching values about 10 times smaller

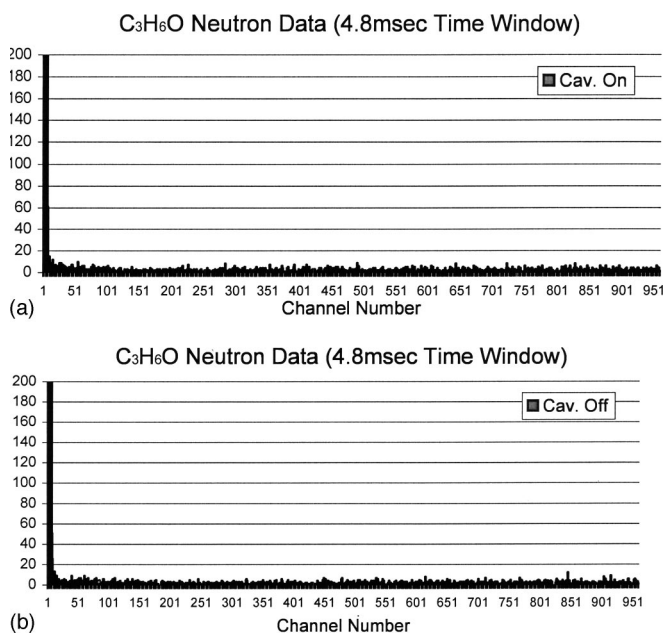


FIG. 5. (a) Time spectrum of neutron counts for tests with cavitation on ( $\text{C}_3\text{H}_6\text{O}$  at  $0^\circ\text{C}$ ; PNG drive frequency  $\sim 200$  Hz; acoustic forcing frequency  $= \sim 20.3$  kHz; time channel width  $= 5 \mu\text{s}$ ). (b) Time spectrum of neutron counts for tests with cavitation off ( $\text{C}_3\text{H}_6\text{O}$  at  $0^\circ\text{C}$ ; PNG drive frequency  $\sim 200$  Hz; PZT drive left on but frequency phase shifted to prevent cavitation onset; time channel width  $= 5 \mu\text{s}$ ).

than in the peak channels. In comparison, the non-cavitation spectrum shown in Fig. 4(b), which was obtained by shifting the phase of the PZT driver, showed a peak lasting  $\sim 15 \mu\text{s}$  from the PNG source neutrons followed by rapidly decreasing neutron counts to a relatively constant background level which persisted out to the end of the sweep at channel 1000 (5 ms). It should be noted that these data trends are consistent with previously reported experimental observations ([www.rpi.edu/~lahey/SciencePaper.pdf](http://www.rpi.edu/~lahey/SciencePaper.pdf)).

We interpret the spectrum of Fig. 4(a) as cavitation-induced neutron production from D-D reactions in the periodically imploding bubble cloud. On the other hand, the non-cavitation spectrum of Fig. 4(b) shows the PNG source neutron peak followed by a rapidly decaying counting rate to channel  $\sim 10$  ( $\sim 50 \mu\text{s}$ ); this decaying count rate is attributed to neutron capture of the PNG source neutrons and possibly the  $\sim 5\%$  of gamma rays which may also be counted when the LS detector is operated in the PSD mode. It is also worth noting that the counting rate in Fig. 4(a) from channels  $\sim 500$  to 1000 remains greater than the background counts in the corresponding region of Fig. 4(b); we interpret this as a small amount of cavitation-induced neutrons from the periodically imploding bubble cloud.

Figures 4(c) and 4(d) present the corresponding time spectra for the cases of cavitation on and off with gating on gamma rays (i.e., we rejected the counts associated with neutrons). As noted therein, the emission spectra do not display the trends observed for neutrons and provide confidence that the spectrum presented in Figs. 4(a) and 4(b) are quite distinct and represent neutron emissions. The aspect of gamma

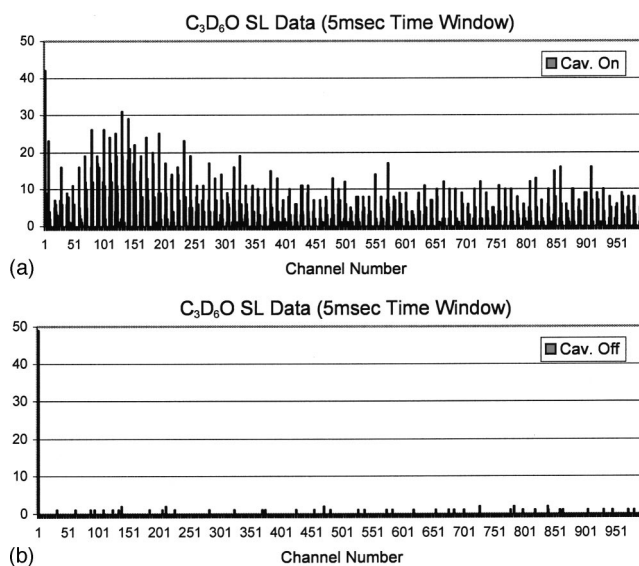


FIG. 6. (a) Typical SL time spectra with cavitation on ( $\text{C}_3\text{D}_6\text{O}$  at  $0^\circ\text{C}$ ; PNG drive frequency  $\sim 200$  Hz; acoustic forcing frequency  $= \sim 19.3$  kHz; time channel width  $= 5 \mu\text{s}$ ). (b) Typical SL time spectra with cavitation off ( $\text{C}_3\text{D}_6\text{O}$  at  $0^\circ\text{C}$ ; PNG drive frequency  $\sim 200$  Hz; PZT drive left on but frequency phase shifted to prevent cavitation; time channel width  $= 5 \mu\text{s}$ ).

ray counts with and without cavitation for deuterated and natural acetone is covered in greater detail in a later section.

As can be seen in Fig. 7(a), the increase of counts (at an overall rate of up to  $\sim 250$  cps) starts about  $30 \mu\text{s}$  after PNG neutron emanation (i.e., during the initial implosion of the bubble cloud which was formed) and the cumulative number of counts, between a  $30 \mu\text{s}$  to  $5000 \mu\text{s}$  time span, was found to be comparable to the counts collected during PNG firing; these counts during bubble implosion varied from run to run between a factor of  $\sim 0.3$  to  $\sim 1.5$  times the total number of neutron counts that were measured for in  $\sim 15 \mu\text{s}$  time bins corresponding to PNG firing, and, as such, they provide an additional useful benchmark for estimating the neutron emission rate due to bubble implosion in  $\text{C}_3\text{D}_6\text{O}$ . The counts during PNG neutron emission were essentially constant from run to run (i.e., well within 1 SD). Assuming Poisson statistics, the change in counts with cavitation that were recorded after PNG operation, for tests with chilled  $\text{C}_3\text{D}_6\text{O}$ , represents a very significant increase of more than 60 SD's [13] above background. Figures 5(a) and 5(b) show, respectively, the neutron count spectrum for the control liquid  $\text{C}_3\text{H}_6\text{O}$  with and without cavitation. These spectra are very similar to Fig. 4(b) and show no evidence of cavitation-induced neutron production.

Figures 6 display representative results for the sonoluminescence (SL) emission spectrum using  $\text{C}_3\text{D}_6\text{O}$ ; the spectrum for  $\text{C}_3\text{H}_6\text{O}$  was found to be similar. As expected, there were no significant SL emission signals unless cavitation bubble implosions took place. Interestingly, however, unlike in Fig. 4(a), there is not a large “dead time” evident in Fig. 6(a). This indicates that the implosions for the first ten or so acoustic cycles after the bubble cloud implosion were not energetic or numerous enough to induce significant DD fu-

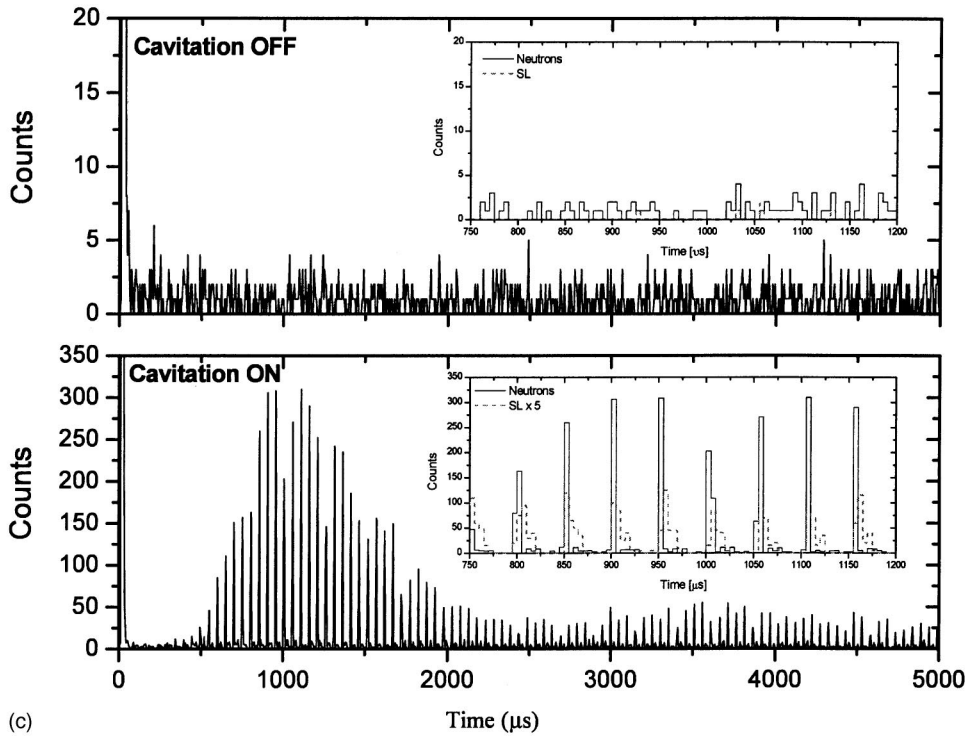
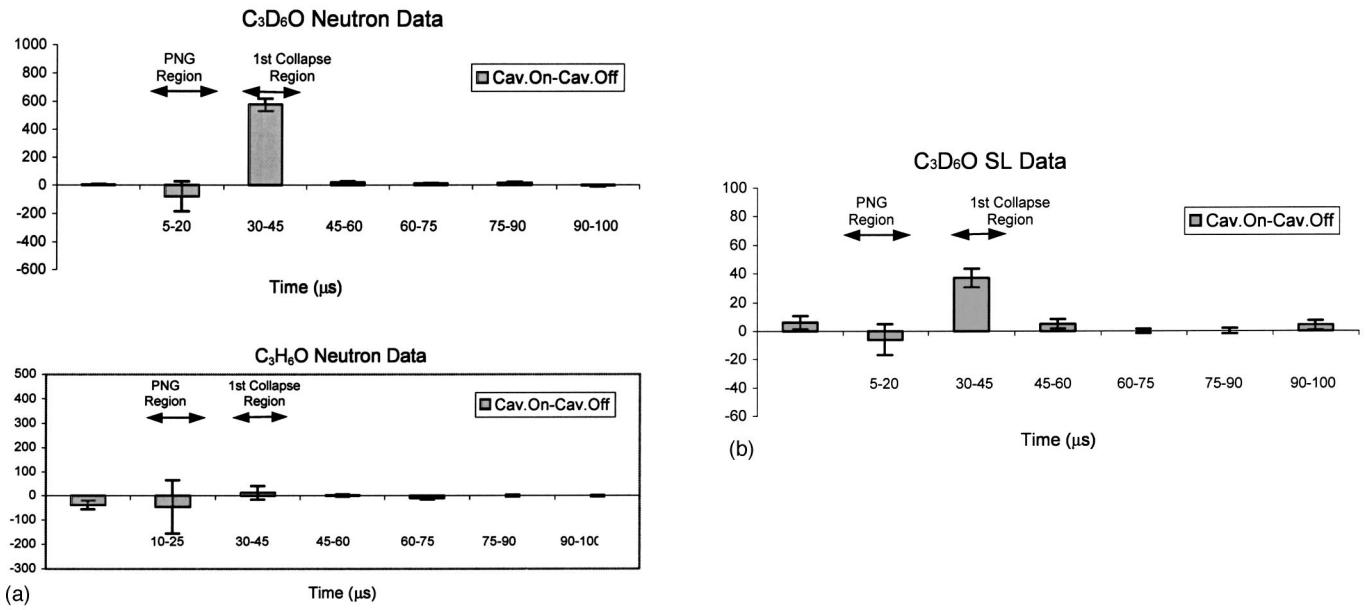


FIG. 7. (a) Change in neutron counts for chilled acetone with cavitation for the first 100  $\mu$ s (acetone at 0  $^{\circ}$ C; PNG drive frequency  $\sim$ 200 Hz; acoustic forcing frequency =  $\sim$ 19.3 kHz; error bars are 1 SD). (b) Corresponding change in SL counts for acetone for first 100  $\mu$ s. (c) Composite plots showing time correlation between neutron and SL counts over 5000  $\mu$ s for cases of cavitation off and cavitation on (C<sub>3</sub>D<sub>6</sub>O at  $\sim$ 0  $^{\circ}$ C; PNG operation at 200 Hz). (d) Time correlation between neutron and SL counts between 0.5 and 2.0 msec. (Cavitation on–cavitation off; C<sub>3</sub>D<sub>6</sub>O at  $\sim$ 0  $^{\circ}$ C; PNG operation at  $\sim$ 200 Hz.) (e) Variation of aggregate neutron and SL counts in peak and in-between peak regions between 0.5 and 2.0 msec. (Cavitation on–cavitation off; C<sub>3</sub>D<sub>6</sub>O at  $\sim$ 0  $^{\circ}$ C; PNG operation at  $\sim$ 200 Hz. Neutron counts per channel in peak channels are about 50 times larger than for remaining channels; the corresponding SL counts per channel in peak channels are about 5 times larger.)

sion, but were able to produce SL light flashes. A plot (for the first 100  $\mu$ s) of the results for neutron and SL activity is shown in Figs. 7(a) and 7(b), respectively. The time correlation of the neutron and SL emissions is evident during the

initial implosion of the bubble cloud. A composite plot of the raw neutron and SL data with cavitation off and cavitation on over the entire 5000  $\mu$ s sweep time is shown in Fig. 7(c). The strong time correlation between neutron and SL emis-



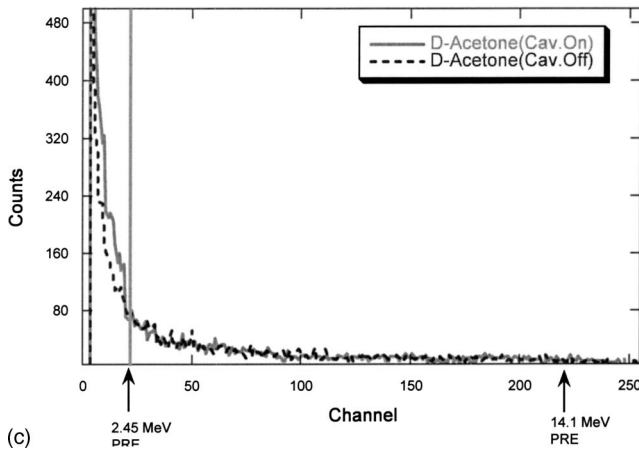
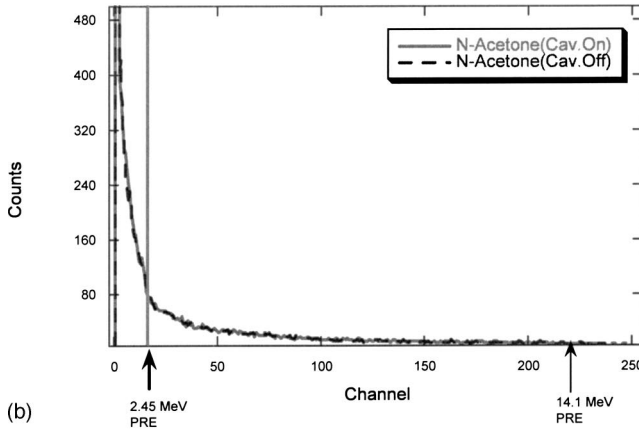
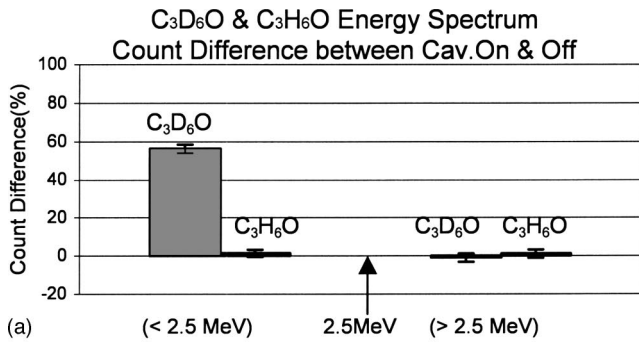


FIG. 8. (a) Changes in neutron counts below and above 2.5 MeV for tests with C<sub>3</sub>D<sub>6</sub>O and C<sub>3</sub>H<sub>6</sub>O at ~0 °C with and without cavitation. (PNG drive frequency=200 Hz. Acoustic drive frequencies = ~19.3 kHz and = ~20.3 kHz for C<sub>3</sub>D<sub>6</sub>O and C<sub>3</sub>H<sub>6</sub>O; error bars are 1 SD.) (b) Representative neutron gated counts below and above 2.5 MeV proton recoil edge (PRE) for tests with C<sub>3</sub>H<sub>6</sub>O at ~0 °C with and without cavitation. (PNG drive frequency =200 Hz. Acoustic drive frequencies = ~20.3 kHz.) (c) Representative neutron gated counts below and above 2.5 MeV proton recoil edge (PRE) for tests with C<sub>3</sub>D<sub>6</sub>O at ~0 °C with and without cavitation. (PNG drive frequency=200 Hz. Acoustic drive frequencies = ~19.3 kHz.)

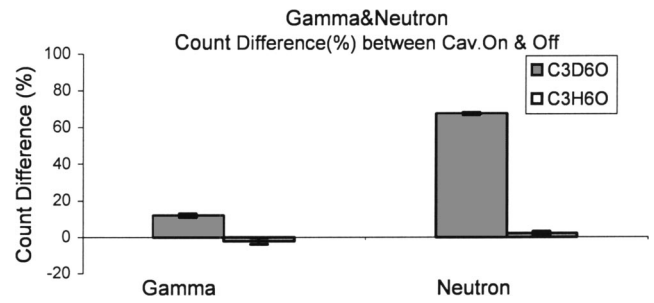


FIG. 9. Changes in gamma ray and neutron counts for tests with C<sub>3</sub>D<sub>6</sub>O and C<sub>3</sub>H<sub>6</sub>O at ~0 °C with and without cavitation. (PNG drive frequency=200 Hz. Acoustic drive frequencies = ~19.3 kHz and = ~20.3 kHz for C<sub>3</sub>D<sub>6</sub>O and C<sub>3</sub>H<sub>6</sub>O; error bars are 1 SD.)

rate varying from  $\sim(1-4) \times 10^5$  n/s (at ~2.5 MeV), which, as will be discussed below, is well within experimental uncertainties for the inferred neutron emission rate of  $\sim(3.5-5) \times 10^5$  n/s from the tritium data.

**GAMMA RAY SPECTRA DATA**

D-D fusion neutrons generated by imploding cavitation bubbles immersed in liquid C<sub>3</sub>D<sub>6</sub>O can be expected to interact with the various surrounding materials and structures resulting in gamma ray emissions (principally from the capture of thermalized neutrons by hydrogen in the liquid scintillator and boron in the Pyrex glass test section). Therefore, to evaluate whether a measurable change in gamma ray emission could be detected, we conducted experiments with and without cavitation for chilled C<sub>3</sub>H<sub>6</sub>O and C<sub>3</sub>D<sub>6</sub>O, obtaining the time and energy spectrum of counts in both the gamma ray and neutron regions. The results, shown in Fig. 9, indicate that for cavitation in chilled C<sub>3</sub>D<sub>6</sub>O the gamma ray counts increased. In various different runs, the increase of gamma ray counts varied from 10% to 20% of the increase in neutron counts. The increase of counts in the neutron region has been noted earlier to be >60 SD. The 10–20 % increase in counts in the gamma region time window amounts to a change of >10 SD which is also very statistically significant. This implies that some of the D-D neutrons emitted are captured by the experimental apparatus. No such change was noted for tests with C<sub>3</sub>H<sub>6</sub>O. Typical C<sub>3</sub>D<sub>6</sub>O gamma ray emission energy spectra with cavitation (less those without cavitation) are shown in Fig. 10. It was found that the increase of gamma ray emissions was mainly (>80%) below 2.2 MeV (as would be expected from the capture of thermalized neutrons by hydrogen and the boron in the Pyrex glass test section). These results confirmed the accompaniment of <2.5 MeV neutrons with a statistically significant emission of gamma rays for cavitation experiments with C<sub>3</sub>D<sub>6</sub>O, but not for tests with the control liquid, C<sub>3</sub>H<sub>6</sub>O.

**CONFIRMATORY TRITIUM EXPERIMENTS**

Following the experimental procedures developed previously [1], additional tests [12] were conducted for seven hours to reconfirm [1] that a statistically significant quantity of tritium (T) was generated during cavitation in chilled

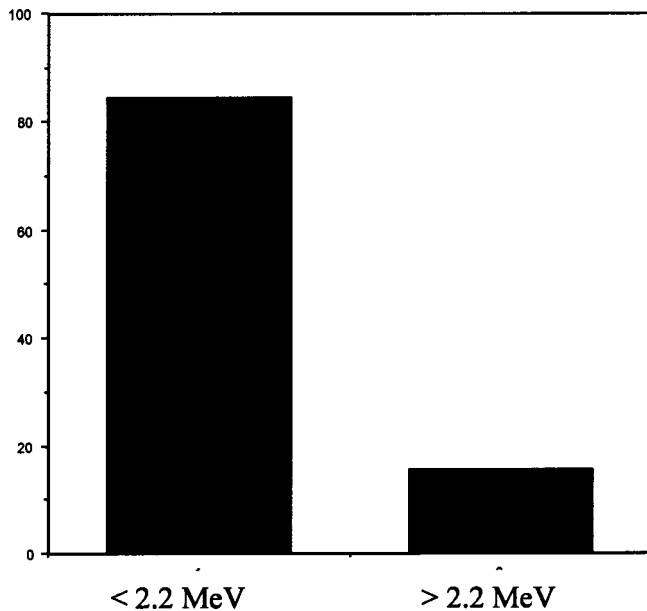


FIG. 10. Increase of sample gamma pulse height spectra fractional distribution of counts above background with cavitation ( $C_3D_6O$  at  $\sim 0^\circ C$ , PNG drive frequency  $\sim 200$  Hz; acoustic drive frequency  $\sim 19.3$  kHz).

$C_3D_6O$  (i.e., at  $\sim 0^\circ C$ ). These tests were conducted with deuterated acetone in a newly fabricated test section, and they confirmed earlier findings [1], and indicated an increase (over background) in tritium counts in the range of 4.5 to 5.9 cpm [with a 1 standard deviation (SD) of about 3 cpm]. This represents an individual difference of up to  $\sim 2$  SD and a collective change of more than 3 SD. These data (i.e., tritium decay at 4.5 to 5.9 cpm) imply an average neutron production rate of between  $\sim 3 \times 10^5$  n/s to  $\sim 5 \times 10^5$  n/s, respectively. Testing in the new chamber with natural acetone ( $C_3H_6O$ ) resulted in a change that was well within 1 SD (i.e., no statistically significant change was found), in agreement with previous findings [1]. For reference, these new confirmatory data are shown together with past data [1] in Fig. 11.

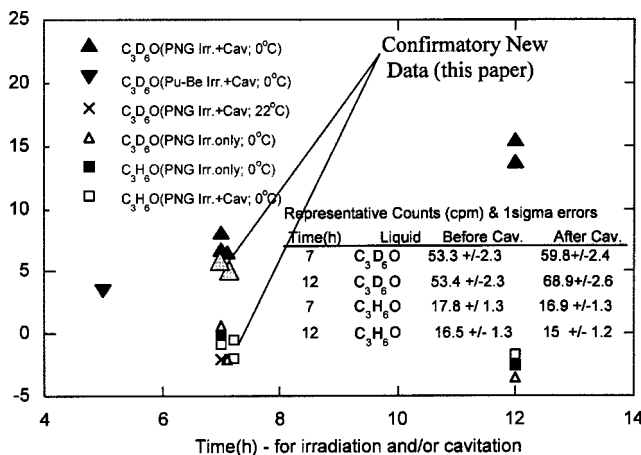


FIG. 11. Confirmatory tritium data together with prior data under similar conditions [1].

To check for possible chemical effects, tests were also conducted using a powerful acoustic horn [12] immersed into  $C_3H_6O$ , and separately into  $C_3D_6O$ , to evaluate whether cavitation of the type produced using conventional means would produce any statistically significant change in the readout for tritium content. The temperature of the acetone was maintained at  $\sim 0^\circ C$  and an acoustic horn operating at an input power level of  $\sim 300$  W was used to induce robust cavitation at 20 kHz. The results revealed a negligible change in counts in samples taken before and after cavitation, amounting to about 0.1 cpm (with 1 SD =  $\sim 3.5$  cpm) for  $C_3D_6O$ , and about 1 cpm (with a 1 SD =  $\sim 2$  cpm) for  $C_3H_6O$ . These changes are well within 1 standard deviation (SD), indicating negligible chemical effects contributing to scintillation activity in the 5 to 18 keV beta decay window characteristic of T decay. These data indicate that the effect of any chemical activity on tritium measurements during cavitation in our experiments is well below that caused by nuclear fusion between deuterium atoms. Therefore, cavitation with SL emanation from deuterated liquids by itself does not lead to an increase of T counts. Indeed, statistically significant quantities of tritium were found to be generated only when we conducted cavitation experiments following the experimental process outlined in Figs. 2 in chilled deuterated acetone ( $C_3D_6O$ ); a finding which was also supported by hydrodynamic shock code simulations [1]. Previously we had also conducted tests with cavitation at liquid temperatures of  $\sim 20^\circ C$  and we did not find any statistically significant change in counts for  $C_3D_6O$  nor  $C_3H_6O$  [1]. Finally, it should be noted that these findings were also supported by hydrodynamic shock code simulations [1].

**SUMMARY AND CONCLUDING REMARKS**

Large and statistically significant emissions of  $\sim 2.5$  MeV and below neutrons were noted during cavitation experiments in chilled deuterated acetone. This neutron emission was well separated in time from the neutrons generated by the PNG (used to nucleate the cavitation bubbles) and was time correlated with SL light emissions during bubble implosion events. The neutron output during cavitation in chilled deuterated acetone was found to be between  $\sim 1 \times 10^5$  n/s and  $\sim 4 \times 10^5$  n/s. Statistically significant increases in tritium were also measured during cavitation of chilled  $C_3D_6O$  and the amount of tritium produced was consistent with the measured DD neutron emissions. Statistically significant gamma ray emissions were also measured in cavitation experiments with chilled  $C_3D_6O$ . No statistically significant change in neutron or gamma ray emissions and no significant tritium generation were observed when there was no cavitation in  $C_3D_6O$  and in control tests with  $C_3H_6O$ , both with and without cavitation.

**ACKNOWLEDGMENTS**

Sponsorship of this research by the Defense Sciences Office of the U.S. Defense Advanced Projects Agency is gratefully acknowledged. We wish to acknowledge the one-on-one in-depth technical involvement, review, comments,

and suggestions for improvement provided by Dr. Jack Harvey of Physics Division, Oak Ridge National Laboratory (ORNL). Additionally, we are grateful to Professor Lee Riedinger, of UT-Battelle, LLC-ORNL and Dr. Glenn Young of Physics Division, ORNL for their in-depth technical reviews and for arranging and coordinating intensive technical reviews over several months by a multitude of scientific staff at ORNL. We further sincerely thank and acknowledge technical reviews by Professor Mark Embrechts and Professor Y. Danon of Rensselaer Polytechnic Institute, Troy, NY, Professor William Bugg, Physics Department and Physics Division jointly of The University of Tennessee, Knoxville, TN and ORNL, Professor Larry Miller of the University of Tennes-

see, Knoxville, TN and ORNL, Dr. Larry Dubois of Stanford Research Institute (previously of DARPA), and Ross Tessien, Dr. Felipe Gaitan, and Dr. William Mead of Impulse Devices, Inc. We also thank Dr. M. Murray, ORNL, for in-depth and direct technical assistance for tritium measurements, and E. Bickel of Channel Industries, Inc., Dr. F. Bergamo of Activations Technologies, Inc., Dr. R. Stevens of Spectrum Techniques, Dr. D. Gedcke of Ortec (Ametek), and Dr. D. Neville of Canberra, Inc. for their valuable advice on nuclear data acquisition. The support and oversight received from Dr. W. Madia of UT-Battelle, LLC-ORNL were also valuable and highly appreciated.

- 
- [1] R. P. Taleyarkhan *et al.*, *Science* **295**, 1868 (2002); R. Nigmatulin, R. T. Lahey, Jr., and R. P. Taleyarkhan, *Science Online*, [www.sciencemag.org/cgi/content/full/295/5561/1868/DC1](http://www.sciencemag.org/cgi/content/full/295/5561/1868/DC1), 2002.
- [2] C. Siefe, *Science* **295**, 1808 (2002).
- [3] F. Bechetti, *Science* **295**, 1850 (2002).
- [4] A. Galonsky, *Science* **297**, 1645 (2002); D. Shapira, M. Saltmarsh, R. P. Taleyarkhan, R. C. Block, C. D. West, and R. T. Lahey, Jr., *ibid.* **297**, 1645 (2002); R. P. Taleyarkhan and S. Putterman (private communication).
- [5] B. Levi, *Phys. Today* **55**(4), 16 (2002).
- [6] D. Shapira and M. Saltmarsh, *Phys. Rev. Lett.* **89**, 104302 (2002).
- [7] The Alpha Spectra LS detector has dimensions of 5 cm (diameter) by 5 cm (length). The scintillation liquid was EJ-301™ which is essentially the same as NE-213™. The test cell (a Pyrex flask  $\sim 200$  mm high  $\times$  65 mm O.D.), with a PZT driver, was designed, fabricated, and set up at ORNL for experiments. The MCA (UCS20™) used was procured from Spectrum Techniques, Oak Ridge, TN, USA; the MCS-PCI™ was procured from Ortec (Ametek), Oak Ridge, TN, USA and the AccuSpec-FMS MCS was procured from Canberra, Inc. SL detection was performed with a (2-ns rise time) PMT.
- [8] N. P. Hawkes *et al.*, *Nucl. Instrum. Methods Phys. Res. A* **476**, 190 (2002).
- [9] G. F. Knoll, *Radiation Detection and Measurement* (Wiley, New York, 1989).
- [10] J. Harvey and N. Hill, *Nucl. Instrum. Methods* **162**, 507 (1979).
- [11] The Pu-Be source used for efficiency and other calibrations emits  $\sim 2 \times 10^6$  n/s, a large fraction of which has energies below 4 MeV. The efficiency of detection of these neutrons by the LS detector located about 18 cm away was found to be  $\sim 2 \times 10^{-4}$ . This efficiency was corrected for the actual distance ( $\sim 7$  cm) of the LS detector from the cavitation region, and by a factor of 2 for the attenuation from interaction with acetone atoms, giving a net detector efficiency of  $\sim 6 \times 10^{-4}$ , a value which is more than ten times greater than the corresponding value reported earlier [1]. This is primarily attributed to the improved detector and electronics used along with a lower bias level. The PNG emitted monoenergetic 14.1 MeV neutrons at a rate that is estimated to lie between  $\sim (5-7) \times 10^5$  n/s. The threshold was set at  $\sim 0.7$  MeV (corresponding to  $\sim 0.7$  MeV proton recoil energy).
- [12] A Beckman LS6500™ scintillation counter, calibrated to detect 5- to 18-keV beta ray decays from T, was used. A 1-cm<sup>3</sup> sample of test liquid was withdrawn from fluid in the top region in the acoustic chamber after testing and mixed with 15 cm<sup>3</sup> of Ecolite™ scintillation cocktail in a borosilicate glass vial. When testing with C<sub>3</sub>D<sub>6</sub>O or C<sub>3</sub>H<sub>6</sub>O, with or without irradiation or cavitation, we used the same experimental configuration, including placing the chamber under standard vacuum conditions. An acoustic horn system (by Misonix™ Corporation) was operated at 20 kHz and half of the  $\sim 660$  W nominal power to result in intense cavitation of the acetone liquid. This power level was about 10 times the power level used to drive the cylindrical PZT affixed to the glass chamber. The tip was immersed into the liquid in the test section which was held under vacuum. A cold air line maintained the temperature of the system at  $\sim 0$  °C.
- [13] In Fig. 4, for the time span after PNG operation (from 30  $\mu$ s to 5000  $\mu$ s), counts collected with and without cavitation were 9869 and 2699, respectively. Assuming Poisson statistics, 1 SD amounts to  $\sqrt{9869+2699} = \sim 112$  counts. Therefore, the 7170 count increase above background represents a change of  $\sim 64$  SD.
- [14] In Fig. 8 the data presented were taken with a Spectrum Techniques UCS20™ MCA in which the background counts from the PNG were included. For the specific discriminator settings and for these test runs with deuterated acetone with and without cavitation, 8347 and 5337 neutrons were counted for the channels below the 2.5 MeV cutoff, with 4193 and 4231 counts above the 2.5 MeV cutoff, respectively. Assuming Poisson statistics, 1 SD amounts to  $\sim 117$  counts. Therefore, the 3010 count increase above background in the  $< 2.5$  MeV range represents a change of  $\sim 26$  SD. Corresponding 1 SD values are shown in Fig. 8 for the various cases cited therein.